Desalination and Water Treatment
www.deswater.com

doi: 10.1080/19443994.2015.1128365

57 (2016) 22061–22073
October

Taylor & Francis
Taylor & Francis Group

Removal of the anionic dye Biebrich scarlet from water by adsorption to calcined and non-calcined Mg–Al layered double hydroxides

Derradji Chebli[a], Abdallah Bouguettoucha[a,*], Abdelbaki Reffas[b], Chafia Tiar[a], Mokhtar Boutahala[a], Holger Gulyas[e], Abdeltif Amrane[c,d]

[a]*Laboratoire de Génie des Procédés Chimiques, Faculté de Technologie, Département de Génie des Procédés, Université Ferhat Abbas, Sétif-1, El Bez, 19000 Sétif, Algérie, Tel./Fax: +213 36 92 51 21; emails: derradji_chebli@yahoo.fr (D. Chebli), abd_bouguettoucha@yahoo.fr (A. Bouguettoucha), chafiatiar@yahoo.fr (C. Tiar), mboutahala@yahoo.fr (M. Boutahala)*
[b]*Laboratoire de Matériaux Inorganiques, Faculté de sciences, Université Mohamed Boudiaf, M'sila, Algérie, email: Abdelbakireffas@gmail.com*
[c]*Ecole Nationale Supérieure de Chimie de Rennes, Université de Rennes 1, CNRS, UMR 6226, Avenue du Général Leclerc, CS 50837, 35708, Rennes Cedex 7, Rennes, France, email: abdeltif.amrane@univ-rennes1.fr*
[d]*Chemistry Department, Universite´ Européenne de Bretagne, Bd Laennec, 35000 Rennes, France*
[e]*Institut für Abwasserwirtschaft und Gewässerschutz, Technische Universität Hamburg-Harburg (TUHH), Eissendorfer Str. 42, D-21073 Hamburg, Germany, email: gulyas@tuhh.de*

Received 13 April 2015; Accepted 1 December 2015

ABSTRACT

A native layered double hydroxide Mg–Al–CO_3, denominated LDH, containing Mg(II) and Al(III) in the layers, was prepared by a co-precipitation method. Its calcined form Mg–Al, (CLDH), was obtained by calcination at 500°C. Both materials were characterized by powder X-ray diffraction (PXRD), Fourier transformation infrared spectroscopy, thermogravimetric analysis, and the determination of the point of zero charge. The porous structure of the solids was investigated by nitrogen adsorption at 77 K. The adsorptive affinity of these materials for Biebrich Scarlet was studied as a function of dye–adsorbent contact time, initial pH of the solution, initial dye concentration, and temperature. Sorption kinetics data fitted best to a pseudo-second-order model suggesting that the process of BS adsorption is controlled by reaction rate for interaction of dye molecules rather than by diffusion. Equilibrium data for both adsorbents were in accordance with both Sips and Langmuir isotherm models. The sorption capacity of CLDH was found to be almost independent on the initial pH, while sorption capacity of LDH was lower in neutral and alkaline conditions than at acidic pH. The adsorption process was also found to be spontaneous and endothermic in nature.

Keywords: Layered double hydroxides; Dye adsorption; Characterization; Kinetics; Isotherms

1. Introduction

Synthetic dyes, which are used in many industrial processes, such as dying of paper, plastics, and fiber, are frequently found in groundwater becoming a serious environmental and public health problem [1]. Remediation of wastewater is a great challenge and has attracted tremendous attention in recent years. Several methods are available for wastewater purification, such as chemical degradation including different

*Corresponding author.

oxidation techniques, biological degradation, photo degradation, coagulation, and membrane filtration [2–5]. Biological processes are usually economically feasible, but many synthetic dyes are recalcitrant toward biological treatment [6]. Physical adsorption is considered to be less expensive within the group of non-biological processes, and it does not generate secondary waste [1]. Many conventional sorbents have been used to remove pollutants from wastewater, such as activated carbon, bentonite, and metal oxides, oxyanions, and oxyhalides [7–9]. However, many of them show low sorption and regeneration efficiencies.

Layered double hydroxides (LDHs) materials, also known as hydrotalcite-like compounds, are a class of anionic layered clays with the general formula $[M(II)_{1-x}M(III)_x(OH)_2]^{x+}(A^{n-}_{x/n})\cdot mH_2O$, where x is typically in the range $0.2 < x < 0.33$, M(II) and M(III) are various di- and trivalent metal cations contained in brucite-like host sheets. A^{n-} represents the interlayer guest anion [10]. Calcination of these LDHs produces non-stoichiometric mixed metal oxides as intermediates, which are characterized by high specific surface areas and homogeneous dispersion of metal cations. An important property of calcined LDHs (CLDH) is the so-called "memory effect," i.e. the calcined products can easily re-establish the original layered structure in an aquatic environment, as expressed by Eq. (1) [11]:

$$Mg_{1-x}Al_xO_{1+x/2} + (x/n)A^{n-} + (m+1+x/2+y)H_2O \rightarrow \left[Mg_{1-x}Al_x(OH)_2\right]^{x+}(A)^{n-}_{x/n}\cdot mH_2O + xOH^- \quad (1)$$

As adsorbents, CLDHs are receiving an increasing interest in the environmental community [11–13], due to their high anion retention capacity and simple thermal regeneration procedure. Although the adsorption behavior of hydrotalcite-type LDHs (both uncalcined and calcined) have been studied by many researchers, the literature dealing with the adsorption behavior of an anionic (acid) dye on LDHs from aqueous solution remains scarce.

The objective of this study was therefore to assess the efficiency of hydrotalcite compounds (calcined and non-calcined) for the adsorption of an anionic azo dye; for this purpose, sodium 6-(2-hydroxynaphthylazo)-3,4′-azodibenzenesulfonate, known as Biebrich Scarlet (BS), was investigated. This molecule (BS) contains two azo groups and two sulphonates functions, it is not biodegradable, and its byproducts are very toxic to the aquatic environment [14]. To our knowledge, adsorption of this azo dye on LDHs has not been previously examined.

The effects of various parameters, namely equilibrium time, initial BS concentration, pH, and temperature on the removal of BS were examined in detail. From experimental data, adsorption isotherms and kinetic models (first-order, pseudo-second-order, and Elovich) were calculated, and adsorption mechanisms were discussed.

2. Materials and methods

2.1. Preparation of dye solutions and adsorbents

BS, $C_{22}H_{14}N_4O_7S_2\cdot 4H_2O$, (Fig. 1), and all other reagents were of analytical grade (p.a.) and used as received without further purification. BS solutions were prepared by dissolving BS in deionized water. For the preparation of the native LDH, an aqueous solution (500 mL) containing NaOH (2 M) and Na_2CO_3 (1 M) was added dropwise to a solution (500 mL) containing $MgCl_2\cdot 6H_2O$ (0.66 M) and $AlCl_3\cdot 9H_2O$ (75.0 g, 0.33 M) (initial Mg/Al ratio = 3.0) under vigorous stirring at constant pH and temperature (pH 10, T = 26 ℃) for 21 h. The precipitate was dried at 65 ℃ for 24 h, ground, and passed through a 100-mesh sieve, giving the LDH product. A fraction of the resulting material was calcined in a muffle furnace at 500 ℃ for 5 h; the solid obtained was denominated as CLDH.

2.2. Characterization of the adsorbents

2.2.1. X-ray diffraction

The LDH and CLDH samples were characterized by the powder X-ray diffraction (PXRD) method, using a Bruker D8 Advance diffractometer operating at 40 kV and 30 mA with CuK radiation (λ = 0.15406 nm).

2.2.2. FT-IR spectroscopy

The FT-IR spectra of the prepared adsorbents were carried out using an FTIR 8400S Shimadzu having a

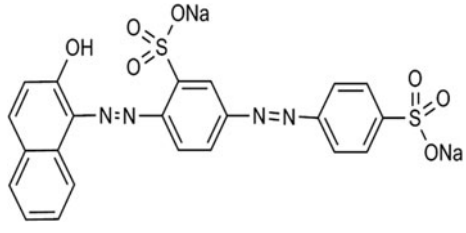

Fig. 1. Molecular structure of BS.

standard mid-IR DTGS detector. Fourier transformation infrared spectroscopy (FTIR) spectra were recorded in the range of 400–4,000 cm^{-1} using the KBr pellets technique.

2.2.3. BET

Nitrogen gas adsorption–desorption isotherms were measured using a Quanta Chrome Autosorb-1 instrument at 77 K. The specific surface area was calculated by the BET method and the pore size was determined by the BJH method using the adsorption and desorption isotherms, respectively. The total pore volume was calculated from the maximum amount of nitrogen gas adsorption at partial pressure $(P/P_0) = 0.999$.

2.2.4. Thermogravimetric analysis

In order to detect the effect on the mass loss of dehydration, dehydroxylation of sheets and formation of mixed oxides, the LDH and CLDH samples were characterized by thermogravimetric analysis (TGA), in an apparatus equipped with Mettler balances with a readability of ±0.1 mg. About 200 mg of sample were heated from 25 to 800˚C with a heating rate of 10˚C min^{-1} under nitrogen flow and the mass was recorded during heating.

2.2.5. Determination of the point of zero charge

The pH_{pzc} was determined by the so-called pH drift method. The pH of a suspension of both CLDH and LDH (50 mg each) and 50 ml of distilled water was adjusted to successive initial values between 2 and 12 with HCl (0.1 M) or NaOH (0.1 M). The suspensions were stirred 24 h and the final pH was measured and plotted versus the initial pH. The pH_{pzc} was determined at the value for which $pH_{final} = pH_{initial}$.

2.3. Sorption experiments

All experiments dealing with dye removal were performed using a batch method by shaking a predetermined amount of adsorbent in 100 ml conical beakers containing 50 ml dye solutions of varying concentrations. After a given contact time for adsorption (24 h) at room temperature, the solid material was separated by centrifugation. The dye concentration was measured at 506 nm wavelength, which corresponds to the maximum absorbance of the BS, using a double-beam Shimadzu spectrophotometer. The adsorption capacity Q_t (mg g^{-1}), representing the amount of adsorbed dye per amount of dry adsorbent at a given time t, was calculated using Eq. (2):

$$Q_t = \frac{(C_0 - C_t)V}{m} \tag{2}$$

where C_0 is the initial dye concentration (mg L^{-1}), C_t is the concentration of dye at any time t, V is the volume of the solution (L), and m is the mass of LDH (mg).

For the evaluation of thermodynamic data, BS adsorption isotherms with both adsorbents were also recorded at 23, 33, 43, and 53˚C. The equilibrium constants, K_C, were calculated according to Eq. (3):

$$K_C = \frac{Q_e}{C_e} \tag{3}$$

2.4. Kinetic experiments

Kinetic studies were conducted to determine the time required for equilibrium establishment and to analyze kinetic models of BS sorption by LDH and CLDH. Batch experiments with a given amount of adsorbent in 50 ml of dye solutions of known concentrations were carried out in a series of 250-ml conical flasks. Suspensions were stirred for different time intervals (5 min to 48 h) at room temperature and then centrifuged. The dye concentration in the supernatants was measured by means of a SAFAS (Monaco 2000) UV–vis spectrophotometer at 480 nm. The adsorbed amounts were determined from the difference between the initial and final concentrations. Impacts of pH (3, 4, 6, and 8), temperature (15, 25, and 35˚C), initial BS concentration C_0 (50, 80, 100, 150, and 250 mg L^{-1}) and adsorbent mass (20, 30, 40, and 50 mg) were investigated.

The dye removal efficiency was calculated by applying Eq. (4):

$$\% \text{ removal} = \frac{(C_0 - C_t)}{C_0} \cdot 100 \tag{4}$$

2.4.1. Equilibrium modeling

Equilibrium data, commonly known as adsorption isotherms, describe how adsorbates interact with adsorbents and hence are critical in optimizing the use of adsorbents. They provide information on the type and capacity of the adsorbent. To analyze the LDH interaction with BS, experimental data

points were fitted to the Langmuir [15], Freundlich [16] and Sips [17] empirical models which are the most frequently used two- and three-parameter equations in the literature describing the non-linear equilibrium between the pollutant adsorbed to the adsorbent particles (Q_e) and the pollutant in solution (C_e) at a constant temperature.

The Langmuir isotherm model assumes uniform energies of adsorption onto the adsorbent surfaces. Furthermore, the Langmuir equation is based on the assumption of the existence of monolayer coverage of the adsorbate at the outer surface of the adsorbent where all sorption sites are identical. The Langmuir equation [15] is given in Eq. (5):

$$\frac{Q_e}{Q_m} = \frac{K_L C_e}{1 + K_L C_e} \tag{5}$$

where Q_e is the equilibrium dye concentration on the adsorbent (mg g^{-1}); C_e is the equilibrium dye concentration in solution (mg L^{-1}); Q_m is the monolayer capacity of the adsorbent (mg g^{-1}); and K_L is the Langmuir constant. A non-linear fit was performed by means of the Origin Software in order to obtain the Langmuir model parameters. The statistic parameter "adjusted R^{2}" was also determined to identify the most accurate model to describe experimental results.

The Freundlich isotherm model assumes neither homogeneous site energies nor limited levels of sorption. The Freundlich model is the earliest known empirical equation and is shown to be consistent with exponential distribution of active centers, characteristic of heterogeneous surfaces [16] (Eq. (6)):

$$Q_e = K_F C_e^{1/n} \tag{6}$$

where Q_e is the equilibrium dye concentration on the adsorbent (mg g^{-1}); C_e is the equilibrium dye concentration in solution (mg L^{-1}); K_F and $1/n$ are empirical constants indicative of sorption capacity and sorption intensity, respectively. The Freundlich parameters were obtained by performing a non-linear fit (Origin software).

The Sips isotherm is a combination of the Langmuir and Freundlich isotherms [17] (Eq. (7)):

$$\frac{Q_e}{Q_m} = \frac{(K_s \cdot C_e)^m}{1 + (K_s \cdot C_e)^m} \tag{7}$$

where Q_m is the maximum monolayer adsorption capacity (mg g^{-1}), K_s is the Sips constant (L mg^{-1}), and m the exponent of the Sips model.

2.4.2. Kinetic modeling

The study of adsorption dynamics describes the solute adsorption rate. This rate controls the residence time of adsorption at the solid–solution interface. Several kinetic models such as pseudo-first-order, pseudo-second-order, and intraparticle diffusion models were applied to fit the experimental data.

2.4.2.1. Pseudo-first-order equation. The pseudo-first-order kinetic model is an equation for the adsorption in a solid/liquid system based on the difference between equilibrium adsorption capacity, Q_e, and actual solid phase concentration, Q_t, measured at a given time t. The linear form of the pseudo-first-order equation is given by Eq. (8) [18]:

$$\ln(Q_e - Q_t) = \ln Q_e - k_1 t \tag{8}$$

where k_1 (1/min) is the equilibrium rate constant of pseudo-first-order equation. The rate constants are obtained from the straight line plots of $\ln(Q_e - Q_t)$ vs. t.

2.4.2.2. Pseudo-second-order equation. The pseudo-second-order model is based on the assumption of chemisorption of the adsorbate on the adsorbent [19]. This model is given by Eq. (9):

$$\frac{t}{Q_t} = \frac{1}{k_2 Q_e^2} + \frac{1}{Q_e} t \tag{9}$$

where k_2 (g mg^{-1} min^{-1}) is the rate constant of pseudo-second-order kinetics. The linear plots of t/Q_t vs. t were used to obtain the rate parameters.

2.4.2.3. Elovich model. The Elovich model [20] results in the linear Eq. (10):

$$Q_t = \frac{1}{\beta} \ln(\alpha \cdot \beta) + \frac{1}{\beta} \ln(t) \tag{10}$$

where α is the initial adsorption rate constant (mg g^{-1} min^{-1})) and the parameter β is related to the extent of surface coverage and activation energy for chemisorption (g mg^{-1}). The values of α and β can be derived from plotting Q_t as a function of $\ln(t)$.

3. Results and discussion

3.1. Characterization of the samples

3.1.1. X-ray diffraction

Fig. 2 shows the XRD patterns of LDH and CLDH. The patterns correspond to hydrotalcite-like compounds with rhombohedral symmetry. The XRD patterns of the LDH (curve b in Fig. 2) fitted well to LDH with basal reflections of planes h k l (0 0 3), (0 0 6), (0 0 9), (0 1 5), (0 1 8), (1 1 0), and (1 1 3) and a basal spacing of 7.52 Å for the reflection (0 0 3). For the calcined hydrotalcite samples, CLDH, a representative PXRD pattern was obtained (diffractogram a in Fig. 2) showing a diffraction which is characteristic of a MgO rock salt structure. In addition, the presence of Al produces a slight shift to a higher angle of the characteristic reflections of MgO assigned to the formation of $Mg_{(1-x)}Al_xO_{(1+x/2)}$ with a rock salt structure [21].

3.1.2. FT-IR spectroscopy

The strong and broad absorption band observed around 3,447 and 3,456 cm^{-1} in both LDH and CLDH spectra before adsorption (Fig. 3) corresponded to the O–H stretching vibration of the layer surface and/or interlayer water molecules. The band at 1,633 and 1,645 cm^{-1} in both spectrum LDH and CLDH spectra, respectively, can be attributed to O–H bending vibration of water molecules. The bands observed in the low-frequency region of the spectrum (<600 cm^{-1}) can be interpreted as lattice vibration modes such as M–O–H vibration and O–M–O stretching [22,23] with M representing Mg or Al.

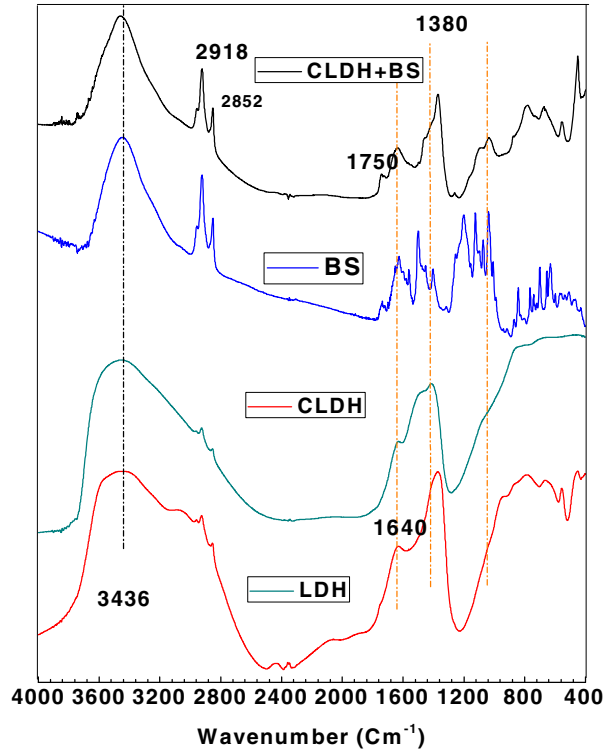

Fig. 3. FTIR spectra of LDH, CLDH, BS, and CLDH+BS.

The absorption bands below 1,000 cm^{-1} were M–O vibration modes of LDH. The spectrum of LDH additionally shows an intense band at around 1,352 cm^{-1} associated with the carbonate ion [24].

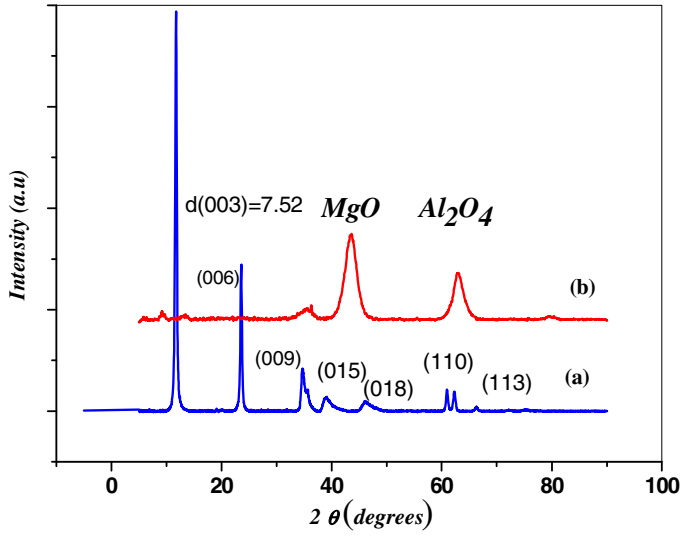

Fig. 2. X-ray diffraction patterns of LDH (a) and CLDH (b).

The shoulder at 3,000 cm^{-1} for LDH might be interpreted as follows: the band at 2,937 cm^{-1} can be assigned to the CO_3–H_2O bridging mode [25]; it can be therefore ascribed to water molecules bound to carbonate ions in the interlayer via hydrogen bonds [26–28]. Thus, it can be concluded that the high intensity of this band (spectrum LDH in Fig. 3) is caused by higher hydration of LDH than that of the CLDH sample (spectrum CLDH in Fig. 3); thus accounting for the single band at 1,352 cm^{-1}. The bands of the CLDH sample in the low-frequency region (below 1,000 cm^{-1}) can be assigned to other vibration modes of carbonate species and to vibrations implying MO, M–O–M, and O–M–O bonds in brucite-type layer.

The shoulder (spectrum LDH) and the band (spectrum CLDH) at 1,415 cm^{-1} in Fig. 3 can be ascribed to the antisymmetric stretching mode of CO_3^{2-} species, recorded as a single band at 1,450 cm^{-1} for free CO_3^{2-} species, which was however split owing to the lower symmetry in the interlayer space, probably due to hydrogen bonding with OH groups and O or H_2O molecules. The values found here for the position of these split bands were very close to those reported by Hernandez-Moreno et al. [29] for Al-Li hydrotalcite materials and by Labajos et al. [27] for Mg–Al hydrotalcite materials. Such a decrease in symmetry also gives rise to assuming the activation of the IR-forbidden V_1 mode of CO_3^{2-} species.

The shoulder at 960 cm^{-1} has been ascribed to the presence of hydroxyl groups [29], while other bands in the 789–450 cm^{-1} range were due to lattice vibrations, mainly involving translation of oxygen ions in the layers. The band found around 450 cm^{-1} corresponded to (MO) vibrations [30].

The FT-IR spectra of the adsorption products are also included in Fig. 3. The strong and broad absorption band observed around 3,445 cm^{-1} corresponded to the O–H stretching vibration of the layer surface and/or interlayer water molecules and the band at 1,633 cm^{-1} was due to O–H bending vibration of water molecules. The bands observed in the low-frequency region of the spectrum (<600 cm^{-1}) can be interpreted as lattice vibration modes such as M–O–H vibration and O–M–O stretching. The absorption peak at 1,372 cm^{-1} was attributed to the υ_3 stretching vibration of CO_3^{2-} [10], indicating the CLDH phase containing some CO_3^{2-}. In the intercalated product, the symmetric sulfonate vibration peak showed same frequency regions (1,091 and 1,035 cm^{-1}) when compared to those of the pure dye salts (1,091 and 1,035 cm^{-1}). This fact indicated that the interactions between the adsorbed dye anions and the hydroxide layers were through the sulfonate groups; the asymmetric sulfonate vibration occurring between 1,130 and 1,184 cm^{-1} for dye salts (BS dye spectra). Also in the FT-IR spectrum of BS, the two strong absorbance peaks at 2,940 and 2,847 cm^{-1} were from the asymmetric and symmetric stretching of CH_2, respectively, while the shoulder peak at 2,960 cm^{-1} was from the asymmetric C–H stretching mode of the terminal CH_3 groups [31]. The BS-CLDH sample showed the characteristic adsorption bonds of BS onto CLDH at 2,922 cm^{-1}, (υ_{as} CH_2), 2,866 cm^{-1}(υ_s CH_2), and 2,960 cm^{-1} (υ_{as} C–H in CH_3). We conclude that after adsorption of this dye onto CLDH, a considerable shifting of the peaks was observed to υ_{as} CH_2 and υ_s CH_2.

3.1.3. BET

Fig. 4(A) shows the N_2 adsorption–desorption isotherms for the LDH and CLDH and their corresponding pore size distributions (PSD) (Fig. 4(B)). The materials exhibited type II isotherms according to the classification of Sing et al. [32], which are typical for mesoporous materials. Isotherms also exhibited an H3-type hysteresis at high relative pressure, which is typical for aggregates of plate-like particles giving rise to slit-shaped pores [33]. This kind of hysteresis is typical of the presence of open large pores, which allow easy diffusion of the reactants through the materials. As seen from Fig. 4(B), the PSD curves were quite broad and bimodal with small mesopores, peak pore at ca. 16 and 22 nm, and larger ones at peak pores 31 and 45 nm for LDH and CLDH, respectively. The smaller mesopores reflect the presence of pores within nanosheets, while larger mesopores can be associated to the pores formed between stacked nanosheets [33]. The inherent mesoporosity of these materials makes them highly suitable to be used as adsorbent for anionic dye molecules having a molecular size dimension between 15 and 30 Å. Table 1 shows the specific surface areas, pore volume, and PSD for the studied solids. The specific surface area of the LDH increased from 58.8 to 131.7 m^2 g^{-1} and the pore volume from 0.022 to 0.0310 cm^3 g^{-1} by heating at 500°C. The removal of water and carbon dioxide during calcination can lead to the formation of channels and pores [34], which are accessible to the nitrogen molecules and could increase the specific surface area of CLDH; showing a. good agreement with the related literature [35].

3.1.4. Thermogravimetric analysis

The TGA plot for the LDH sample (Fig. 5) shows weight losses in three distinct temperature ranges: 25–225, 225–450, and 450–800°C. The weight loss in the first step (25–225°C) was about 38.1% which is

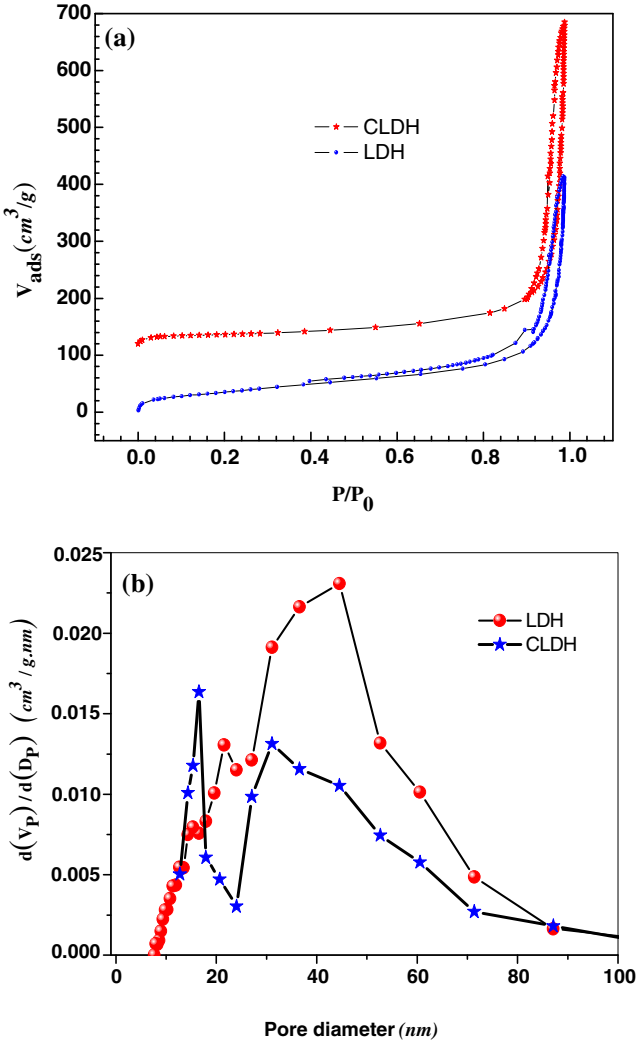

Fig. 4. Adsorption–desorption isotherms of N_2 of LDH and CLDH (a) and pore distribution of LDH and CLDH (b).

Table 1
BET surface and porosity parameters obtained from N_2 adsorption of LDH and CLDH samples

	S_{BET} (m^2/g)	Vp (cm^3/g)	Dp (nm)
LDH	58.8	0.022	22 and 45
CLDH	131.7	0.031	13 and 31

a common characteristic of hydrotalcites related to the loss of physisorbed and interlayer water. The second weight loss (52.4%), which occurred between 225 and 450°C, was due to the first step of dehydroxylation and the removal of carbonate ions from the interlayer. In this temperature range, metal oxides were formed. In the third range, final mass loss (about 9.5%) occurring beyond 450°C, continued dehydroxylation

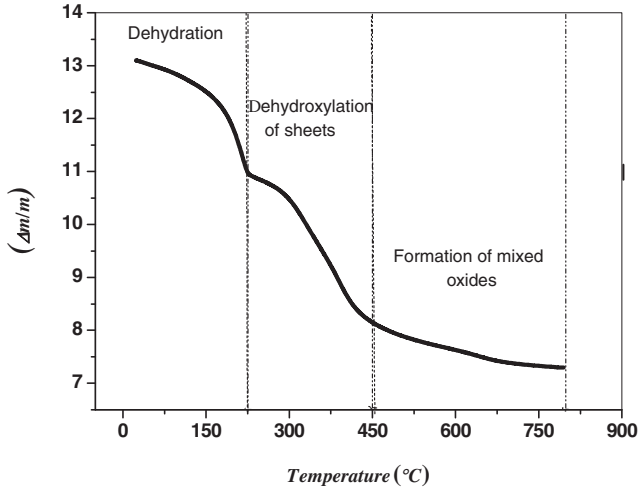

Fig. 5. TGA plot of LDH.

and decarbonatation took place forming more metal oxides such as MgO, which was detected in the X-ray diffractogram of LDH (uncalcined hydrotalcite), and probably $MgAl_2O_4$ as reported by Ferreira et al. [36]. At higher temperatures, the material becomes an amorphous metastable mixed solid oxide. The total weight loss of the pure sample in the temperature range up to 450°C was approximately 91% (Fig. 5), which corresponds to the sum of water and carbonate contents.

3.2. Adsorption experiments

3.2.1. Effect of pH on dye sorption

The pH is an important parameter controlling the solid–liquid interface. Fig. 6 shows the plots of adsorption capacity vs. initial pH ranging from 3 to 11 for CLDH and LDH. The dye adsorption on LDH decreased with increasing the initial pH from 5 to 7.

The effect of pH on dye adsorption by LDH can be explained in terms of the point of zero charge (PZC) and the pK_a of the dye. The PZC is the pH where the net total particle charge is zero. The PZC can be used as a qualitative parameter for the adsorbent surface charge balance.

The PZC were 12 and 10 for CLDH and LDH, respectively (Fig. 7). Along with the positive charge that results from isomorphic substitution, LDH has variable charges that result from the adsorption of ions from the solution, such as H^+ or OH^- [37].

For pH values below the PZC:

$$\text{Sur–OH} + H_3O^+ \rightarrow \text{Sur–}OH_2^+ + H_2O \quad (11)$$

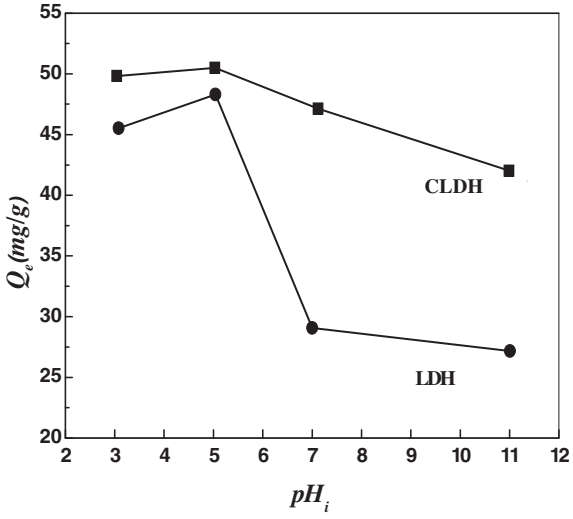

Fig. 6. Effect of initial pH on the adsorption of dye by (a) LDH and (b) CLDH (C_0 = 50 mg/L, T = 23°C).

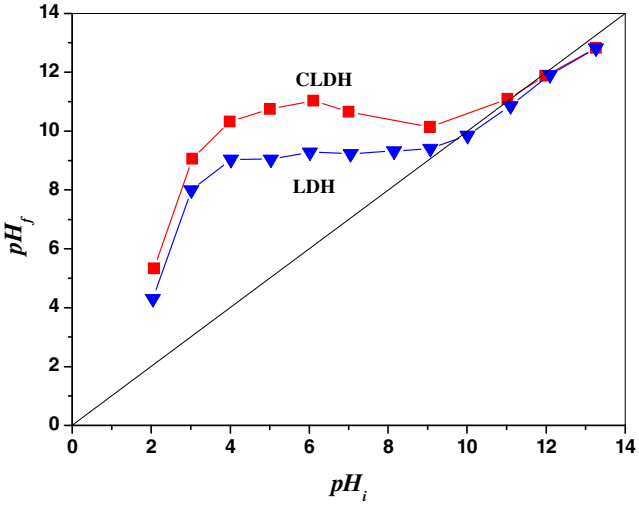

Fig. 7. The change in pH_{final} as a function of $pH_{initial}$ in the LDH and CLDH suspensions in water during the determination of the PZC.

For pH values above the PZC:

$$Sur–OH + OH^- \rightarrow Sur–O^- + H_2O \quad (12)$$

where "Sur" denotes the surface of LDH and CLDH.

For pH values below the PZC, the hydrated surface of the LDH is protonated and thus positively charged, while it is deprotonated and hence negatively charged at pH values above the PZC.

Besides deprotonation of the surface hydroxyl groups as mentioned above, exchange of carbonate anions in the interlayer by hydroxide anions from the solution takes place [38]. In aqueous solution, the sulfonate groups of the dissolved BS dye (D-SO_3Na) are dissociated and converted to anionic functional groups [39,40] as given in Eq. (13):

$$D–SO_3Na \rightarrow D–SO_3^- + Na^+ \quad (13)$$

The extent of dissociation of the two sulfonic acid groups is described by the pK_a. Sulfonic acid groups of BS are assumed to be strongly dissociated even at low pH. At pH values below the PZC of the adsorbent, there may be two possible mechanisms for dye adsorption: one of them is anionic exchange of CO_3^{2-} anions in the interlayer by dye anions (D-SO_3^-). The anionic dye is in competition with the OH^- in the solution for exchange with the CO_3^{2-} anions that are associated with the surface. The other mechanism is adsorption by means of association between the positively charged surface (Sur—OH_2^+) of LDH and the dye anions. For pH values above the PZC, there is a decrease of both, the deprotonation of surface hydroxyls groups and the positive charge on the surface of LDH, leading to a decrease in dye removal.

The above explanations appear in agreement with the experimental curve profile (Fig. 6) and hence for the increased amount of adsorbed anionic dye in acidic conditions.

However, a significant decrease in dye adsorption below pH 5.0 (at pH 3.0) may result from the dissolution of the Mg–Al–CO_3 structure of LDH, which was also observed in other studies [37]. At the same time, dye adsorption (below pH 5.0) on CLDH might also be slightly increased by decreasing OH^- concentration at the surface of the CLDH. Therefore, the adsorbed amount of dye decreased in the case of LDH. For acid solutions (pH ≤ 5), the protons from the aqueous solution make the surface of the adsorbent positive, thus promoting electrostatic attraction between the surface and the sulfonate groups (usually negatively charged) of the azo dye molecules in the solution [41].

3.2.2. Effect of contact time and initial concentration

Adsorption experiments to evaluate the contact time effect on BS removal by both non-LDH and CLDH were carried out for 8 h, at 296 K, pH 5.0, and for dye concentrations ranging from 50 to 400 mg L^{-1}. The plots (Fig. 8) show that the adsorbed amount was lower on LDH than on CLDH for the same initial dye concentration. The percentage of BS removal decreased with increasing initial BS concentration from 72.3 to 46.2% for 100 mg L^{-1} BS to 43.6 and 27.6% for 200 mg L^{-1} BS

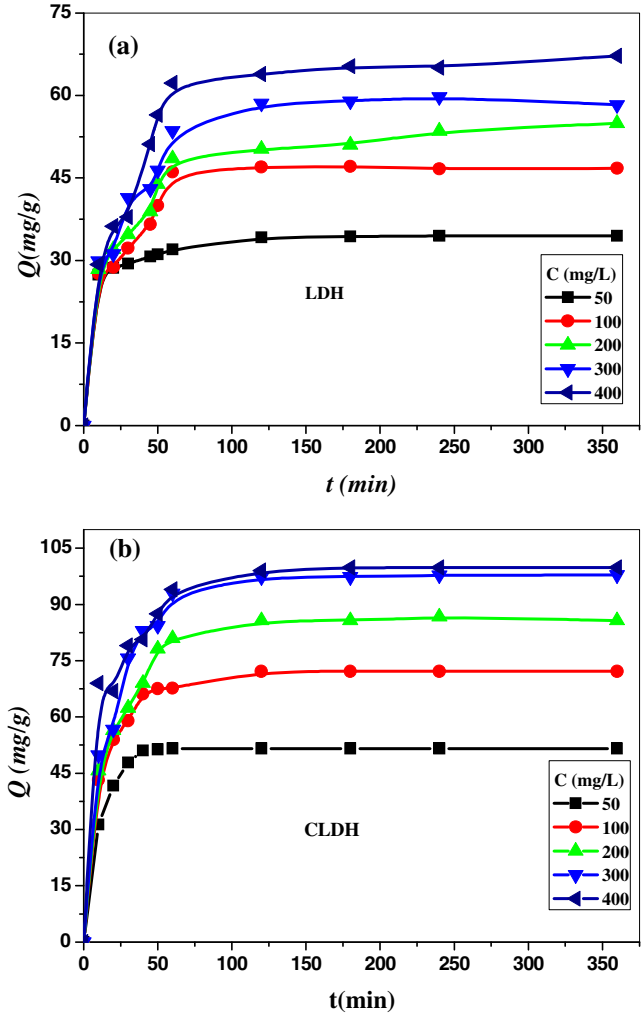

Fig. 8. Effect of the contact time and initial BS concentration on the adsorption capacity of BS onto (a) LDH and (b) CLDH (T = 23°C, agitation speed = 200 rpm, pH 5).

for CLDH and LDH, respectively (Fig. 8). BS adsorption took place very quickly, achieving equilibrium in all cases within about 100 and 150 min of experiments for LDH and CLDH, respectively. The initial dye concentration had no pronounced effect on the equilibrium time. To account for the difference between equilibrium time obtained with LDH and CLDH (t_{eqLDH} = 130 min < t_{eqCLDH} = 175 min), it can be suggested that dye adsorption on LDH may occur via exchange mechanism, while for CLDH it occurs probably by both surface and ion-exchange phenomena by layer reconstruction (memory effect) [40].

3.3. Isotherm modeling

In order to optimize the design of an adsorption system, it is important to establish the most appropriate

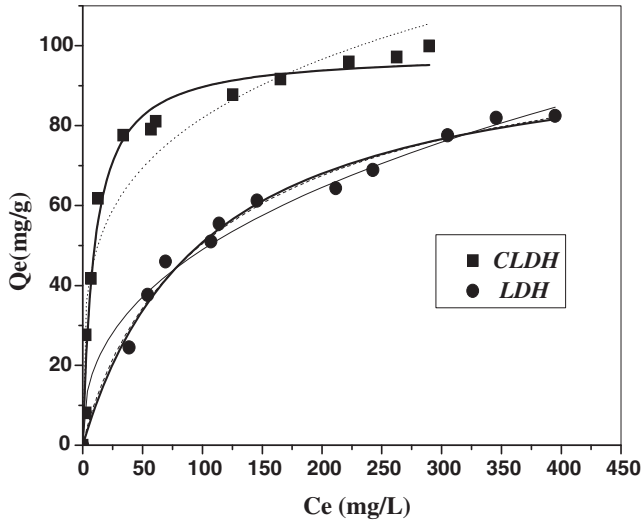

Fig. 9. Experimental (symbols) and calculated isotherm data (lines) for BS adsorption to NLDH and CLDH, normal lines: Langmuir; dot lines: Freundlich; dashed lines: Sips (T = 23°C, C = 50 mg/l, V = 50 ml, 200 rpm, pH 5).

correlation for the equilibrium curve. Several equilibrium adsorption isotherm models are available, and the most common ones are the monolayer adsorption developed by Langmuir, the multilayer adsorption of Freundlich and the Sips isotherm. Experimental data of BS adsorption on both CLDH and LDH were fitted to the isotherm models using Origin software. The graphical representations of these models are presented in Fig. 9 and all constants are summarized in Table 2. Although all models represented good estimations for

Table 2
Langmuir, Freundlich, and Sips constants for the adsorption of BS on LDH and CLDH

Model		CLDH	LDH
Experimental	Q_{exp} (mg/g)	99.94	82.43
	Q_m (mg/g)	98.33	102.7
Langumuir	K_L (L/mg) × 10^3	0.104	0.009
	R^2	**0.98**	**0.98**
	n_F	2.5	4.16
	$1/n_F$	0.40	0.24
Freundlich	K_F (mg/g)	7.81	27.34
	R^2	**0.91**	**0.98**
	Q_m (mg/g)	98.4	110.41
Sips	K_{LF}	0.103	0.008
	m_{LF}	1.00	0.90
	R^2	**0.98**	**0.99**

Notes: The values were highlighted in bold in order to illustrate the best and fitting model.

Table 3
Parameters of kinetic models for the adsorption of BS (T = 23°C, pH 5)

Pseudo-first-order						Pseudo-second-order				Elovich Model		
CLDH	C (mg/L)	Q_{exp} (mg/g)	Q_e (mg/g)	k_1 (min^{-1})	R^2	Q_{exp} (mg/g)	Q_e (mg/g)	k_2 (g/mg. min)	R^2	α (mg/g min)	β (g/mg)	R^2
	50	51.58	66.71	0.112	**0.96**	51.58	59.73	2	**0.99**	12.85	0.069	**0.99**
	100	72.18	59.29	0.055	**0.96**	72.18	78.06	1.5	**0.99**	24.91	0.064	**0.98**
	200	85.71	75.29	0.042	**0.94**	85.71	90.13	0.071	**0.98**	19.71	0.052	**0.94**
	300	97.9	83.93	0.040	**0.94**	97.9	102.43	0.052	**0.97**	17.27	0.041	**0.90**
	400	99.86	67.35	0.035	0.81	99.86	105.18	1.1	**0.97**	15.48	0.070	**0.83**
LDH	50	34.72	16.14	0.0357	**0.74**	34.72	35.32	0.53	**0.99**	15.12	0.406	**0.95**
	100	47.1	48.91	0.0495	**0.73**	47.1	52.79	0.3	**0.98**	13.05	0.106	**0.75**
	200	54.94	47.94	0.0449	**0.82**	54.94	56.27	0.12	**0.98**	12.79	0.096	**0.83**
	300	58.58	51.41	0.033	**0.88**	58.58	67.29	0.07	**0.98**	10.96	0.079	**0.83**
	400	67.22	76.7	0.0525	**0.82**	67.22	75.75	0.065	**0.97**	7.485	0.055	**0.85**

Notes: The values were highlighted in bold in order to illustrate the best and fitting model.

both CLDH and LDH, the Sips and the Langmuir models led to the best estimations for adsorption to CLDH with a correlation coefficient R^2 close to 1 (Table 2).

3.4. Kinetics modeling

Generally, three steps are involved during the process of adsorption by porous adsorbent particles: external mass transfer, intraparticle transport, and chemisorption. Pseudo-first-order pseudo-second-order, and Elovich models [41], were tested to fit experimental adsorption data.

For both investigated adsorbents, the pseudo-second-order model appeared to lead to the most accurate fit of experimental data (Table 3). For the LDH adsorbent, both the pseudo-first-order model and the Elovich model did not result in an accurate description of experimental data, since correlation coefficients (R^2) were below 0.90 for most of the investigated initial BS concentrations (Table 3). In addition to the high R^2 values (>0.99 for all tested conditions), the Q_e values estimated from the pseudo-second-order kinetic model were also in agreement with the experimental values, Q_{exp}, for all tested concentrations (Table 3) and Fig. 10 shows the linear fits for the pseudo-second-order kinetics according to Eq. (10). The results suggested that boundary layer resistance was not the rate-limiting step since dye adsorption followed pseudo-second-order kinetic [42].

3.5. Thermodynamic analysis

The thermodynamic parameters reflect the feasibility and the spontaneous nature of a sorption process. Parameters such as the free energy change (ΔG), the enthalpy change (ΔH), and the entropy change (ΔS)

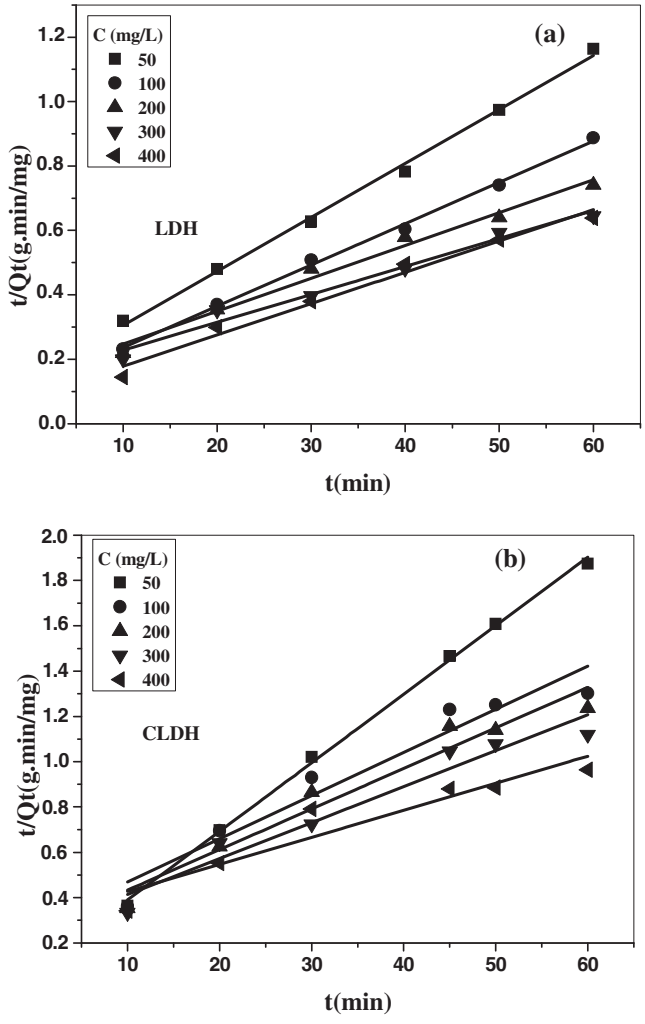

Fig. 10. Experimental (symbols) and calculated data (continuous lines) by means of pseudo-second-order kinetic model for BS adsorption onto (a) LDH and (b) CLDH (T = 23°C, agitation speed = 200 rpm, pH 5).

Table 4
Thermodynamic parameters for the adsorption of BS on LDH and CLDH

	Temperature (K)	K_c 10^{+3} (L/g)	ΔH° (kJ/mol)	ΔS° (J/mol·K)	ΔG° (kJ/mol)
	296	1.17			−1.36
LDH	306	2.01	14.49	53.55	−1.98
	316	2.52			−2.43
	326	3.04			−2.97
	296	2.52			−2.04
CLDH	306	3.23	24.86	90.87	−2.95
	316	4.82			−3.85
	326	6.15			−4.76

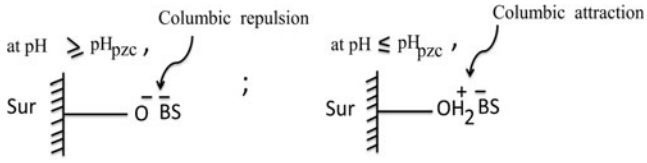

Fig. 11. Schematic representation of possible adsorption mechanism of BS at pH ≥ pHpzc and pH ≤ pHpzc.

can be estimated considering the variations in the equilibrium constants with the temperature. The free energy change of the adsorption reaction is given using Eq. (14) as reported by Milonjic [43] and Reffas et al. [44]:

$$\Delta G^\circ = -RT\ \ln(\rho K_C) \tag{14}$$

$$K_C = \frac{Q_e}{C_e} \tag{3}$$

where ΔG° is the free energy change (kJ mol^{-1}), R is the universal gas constant (8.314 J mol^{-1} K^{-1}), T is the absolute temperature (K), K_C is the thermodynamic equilibrium constant (L g^{-1}), and ρ is the water density (g L^{-1}). ΔH° and ΔS° values of the adsorption process were determined from the Van't Hoff equation (Eq. (15)):

$$\ln(\rho K_C) = -\frac{\Delta H}{RT} + \frac{\Delta S}{R} \tag{15}$$

ΔH and ΔS can be deduced from the slope ($\Delta H/R$) and the intercept ($\Delta S/R$) of the plot of $\ln(\Delta K_c)$ vs. $1/T$. The calculated thermodynamic parameters are given in Table 4.

The negative values of ΔG° irrespective of the considered temperature illustrated the spontaneous nature of the adsorption; the positive value of ΔH° suggested its endothermic nature and the positive value of ΔS° suggested an increasing randomness at the solid–solution interface during the adsorption of BS on CLDH.

3.6. Proposed mechanisms of adsorption

Understanding the mechanism of anionic dye adsorption on solid LDH surface is essential for effective removal of dyes from textile wastewaters. The mechanisms of the dye adsorption onto LDH were investigated using FTIR technique. The LDH surface contains hydroxide groups, which are very reactive group, and can react with many polar organic compounds and various functional groups. LDH has variable charges that result from the adsorption of ions from the solution, such as H^+ or OH^-; for pH values below the PZC (Eq. (11)) and above the PZC (Eq. (12)). FTIR offers some indication about the ability of this dye to react with hydroxide groups of the surface of LDH. Fig. 3 shows that when the dye was adsorbed on CLDH, the peak shifts from 1,415 cm^{-1} (antisymmetric stretching mode of CO_3^{2-}) to 1,372 cm^{-1} (υ_3 stretching vibration of CO_3^{2-}). According to the FTIR spectra and the pH dependency of the adsorption of BS, there was an electrostatic (columbic) attraction between BS and the positive charge on the surface of CLDH at pH below 5 (i.e. pH ≤ 5) (Sur—OH_2^+ D-SO_3^-); while for pH values above 5 (pH ≥ 5), there was an electrostatic (columbic) repulsion between BS and the negative charge on the surface of CLDH, leading to a decrease in dye removal. Consequently, the mechanism proposed can be illustrated in Fig. 11.

4. Conclusion

The adsorption quantity of eliminated BS depends on the physical characteristics (crystallinity and PSD) of the precursor Mg–Al–CO_3 LDH and the calcined

product (CLDH) used as adsorbent. Under the studied conditions, CLDH was obviously a more effective material for BS adsorption as the experimentally determined maximum adsorptive capacities were 99.9 and 82.4 mg L^{-1} for CLDH and LDH, respectively. However, the maximum adsorption capacities Q_{max} calculated from Langmuir adsorption isotherms were 102.7 and 98.3 mg g^{-1} for LDH and CLDH, respectively.

The adsorption of the acid BS on the calcined sample may have took place on the external surface as well as in the interlayer space through a reconstruction process following pseudo-second-order kinetics. The Langmuir and the Sips isotherm models accurately described experimental data with high determination coefficients. The negative values for the Gibbs free energy ΔG° indicate that the dye adsorption process on calcined and non-calcined LDH was spontaneous, endothermic in nature, and enhanced when the temperature was increased from 23 to 53˚C. The enthalpy values indicated that the interaction type is a combination of physical and chemical adsorption due to the adsorption on the external surface of the adsorbents and dye interaction in the interlayer space of the LDHs. The adsorption of BS on LDH reached equilibrium after ≤150 min and the dye removal increased with decreasing pH.

Both LDHs materials show therefore a high potential for dye removal. The calcined material appeared to be more efficient as compared to LDH; it showed larger adsorption capacities at low BS equilibrium concentrations in the liquid phase. It is therefore an excellent candidate to substitute activated carbon, which is more expensive than LDH materials.

References

[1] H.S. Reife Freeman, in: A. Reife, H.S. Freeman (Eds.), Environmental Chemistry of Dyes and Pigments, Wiley, New York, NY, 1996.

[2] M. Ghaedi, A. Hassanzadeh, S. Naciri Kokhdan, Multiwalled carbon nanotubes as adsorbents for the kinetic and equilibrium study of the removal of alizarin red S and morin, J. Chem. Eng. Data 56 (2011) 2511–2520.

[3] Z. Yao, L. Wang, J. Qi, Biosorption of Methylene blue from aqueous solution using a bioenergy forest waste: Xanthoc-eras sorbifoliaseed coat, Clean 37 (2009) 642–648.

[4] M.M. Abd EI-Latif, A.M. Ibrahim, M.F. EI-Kady, Adsorption equilibrium, kinetics and thermodynamics of Methylene blue from aqueous solutions using biopolymer oak sawdust composite, J. Am. Sci. 6 (2010) 267–283.

[5] V. Vimonses, S. Lei, Kinetic study and equilibrium isotherm analysis of Congo Red adsorption by clay materials, Chem. Eng. J. 148 (2009) 354–364.

[6] V.M. Correia, T. Stephenson, S.J. Judd, Characterisation of textile wastewaters—A review, Environ. Technol. 15 (1994) 917–929.

[7] A. Sultana, Equilibrium and kinetic evaluation of the adsorption of commercial brilliant red on used black tea leaves, MS Thesis, University of Dhaka, Bangladesh, (2006).

[8] S. Bailey, T.J. Olin, R.M. Bricka, D. Adrian, A review of potentially low-cost sorbents for heavy metals, Water Res. 33 (1999) 2469–2479.

[9] D. Chebli, A. Bouguettoucha, T. Mekhalef, S. Nacef, A. Amrane, Valorization of an agricultural waste, *Stipa tenassicima* fibers, by biosorption of an anionic azo dye, Congo red, Desalin. Water Treat. 54 (2015) 245–254.

[10] F. Cavani, F. Trifirò, A. Vaccari, Hydrotalcite-type anionic clays: Preparation, properties and applications, Catal. Today 11 (1991) 173–301.

[11] A.R. Auxilio, P.C. Andrews, P.C. Junk, L. Spiccia, D. Neumann, W. Raverty, N. Vanderhoek, Adsorption and intercalation of Acid Blue 9 on Mg–Al layered double hydroxides of variable metal composition, Polyhedron 26 (2007) 3479–3490.

[12] V.R.L. Constantino, T.J. Pinnavaia, Basic properties of $Mg^{2+}_{1-x}Al^{3+}_{x}$-layered double hydroxides intercalated by carbonate, hydroxide, chloride, and sulfate an-ions, Inorg. Chem. 34 (1995) 883–892.

[13] G.S. Thomas, A.V. Radha, P.V. Kamath, S. Kannan, Thermally induced polytype transformations among the layered double hydroxides (LDHs) of Mg and Zn with Al, J. Phys. Chem. B 110 (2006) 12365–12371.

[14] D. Chebli, Traitement des eaux usées industrielles: Dégradation des colorants azoïques par un procédé intégré couplant un procédé d'oxydation avancée et un traitement biologique (Industrial wastewater treatment: Azo dyes removal by means of an integrated process coupling an advanced oxidation process and a biological treatment), Université de SETIF, Février, Thèse de Doctorat, 2012.

[15] I. Langmuir, The adsorption of gases on plane surfaces of glass, mica and platinum, J. Am. Chem. Soc. 40 (1918) 1361–1403.

[16] H.M.F. Freundlich, Ober dies adsorption in Losungen (Regarding adsorption in solution), Z. Phys. Chem. 57 (1906) 385–470.

[17] G.L. Dotto, M.L.G. Vieira, V.M. Esquerdo, L.A.A. Pinto, Equilibrium and thermodynamics of azo dyes biosorption onto *Spirulina platensis*, Braz. J. Chem. Eng. 30 (2013) 13–21.

[18] S. Lagergren, Zur Theorie der sogenannten Adsorption gelöster Stoffe (On the theory of so-called adsorption of solutes), K. Sven. Vetenskapsakad. Handl. 24 (1898) 1–39.

[19] V.C. Srivastava, I.D. Mall, I.M. Mishra, Adsorption of toxic metal ions onto activated carbon, Chem. Eng. Process. Process Intensif. 47 (2008) 1269–1280.

[20] S.H. Chien, W.R. Clayton, Application of Elovich equation to the kinetics of phosphate release and sorption on soils, Soil Sci. Soc. Am. J. 44 (1980) 265–268.

[21] V. Rives, Layered Double Hydroxides: Present and Future, Nova Science (Ed.), Publishers, Inc., New York, NY, 2001.

[22] Q. Wang, Y. Feng, J. Feng, D. Li, Enhanced thermal- and photo-stability of acid yellow 17 by incorporation

into layered double hydroxides, J. Solid State Chem. 184 (2011) 1551–1555.
[23] P. Tang, Y. Feng, D. Li, Improved thermal and photostability of an anthraquinone dye by intercalation in a zinc–aluminum layered double hydroxides host, Dyes Pigm. 90 (2011) 253–258.
[24] R.M. Queiroz, L.H.O. Pires, R.C.P. de Souza, J.R. Zamian, A.G. de Souza, G.N. da Rocha Filho, C.E.F. da Costa, Thermal characterization of hydrotalcite used in the trans esterification of soybean oil, J. Therm. Anal. Calorim. 97 (2009) 163–166.
[25] L. Hickey, J.T. Kloprogge, R.L. Frost, The effects of various hydrothermal treatments on magnesium–aluminium hydrotalcites, J. Mater. Sci. 35 (2000) 4347–4355.
[26] E.C. Kruissink, L.L. van Reijen, J.R.H. Ross, Coprecipitated nickel–alumina catalysts for methanation at high temperature. Part 1. Chemical composition and structure of the precipitates, J. Chem. Soc., Faraday Trans. 1: Phys. Chem. in Condensed Phases 77 (1981) 649–663.
[27] F.M. Labajos, V. Rives, M.A. Ulibarri, Effect of hydrothermal and thermal treatments on the physicochemical properties of Mg–Al hydrotalcite-like materials, J. Mater. Sci. 27 (1992) 1546–1552.
[28] D.L. Bish, G.W. Brindly, A reinvestigation of takovite, a nickel aluminum hydroxyl carbonate of the pyroaurite group, Am. Miner. 62 (1977) 458–464.
[29] J.M. Hernandez-Moreno, M.A. Ulibarri, J.L. Rendon, C.J. Serna, IR characteristics of hydrotalcite-like compounds, Phys. Chem. Miner. 12 (1985) 34–38.
[30] E. Uzunova, D. Klissurski, S. Kassabov, Nickel–iron hydroxide carbonate precursors in the synthesis of high-dispersity oxides, J. Mater. Chem. 4 (1994) 153–159.
[31] M. Islam, Z. Guo, D. Rutman, T. Benson, Immobilization of triazabicyclodecene in surfactant modified Mg/Al layered double hydroxides, RSC Adv. 3 (2013) 24247–24255.
[32] K.S.W. Sing, D.H. Everett, R.A.W. Haul, L. Moscou, R.A. Pierotti, J. Rouquerol, T. Siemieniewska, Reporting physisorption data for gas solid systems with special reference to the determination of surface area and porosity (recommendations 1984), Pure Appl. Chem. 57 (1985) 603–619.
[33] J. Zhou, S. Yang, J. Yu, Z. Shu, Novel hollow microspheres of hierarchical zinc–aluminum layered double hydroxides and their enhanced adsorption capacity for phosphate in water, J. Hazard. Mater. 192 (2011) 1114–1121.
[34] Z. Yu, D. Chen, M. Rønning, T. Vrålstad, E. Ochoa-Fernández, A. Holmen, Large-scale synthesis of carbon nanofibers on Ni–Fe–Al hydrotalcite derived catalysts, Appl. Catal. A: Gen. 338 (2008) 136–146.
[35] O.W. Perez-Lopez, A. Senger, N.R. Marcilio, M.A. Lansarin, Effect of composition and thermal pretreatment on properties of NiMgAl catalysts for CO_2 reforming of methane, Appl. Catal. A: Gen. 303 (2006) 234–244.
[36] O.P. Ferreira, O.L. Alves, D.X. Gouveia, A.G. Souza Filho, J.A.C. de Paiva, J. Mendes Filho, FilhoThermal decomposition and structural Reconstruction effect on Mg–Febased hydrotalcite compounds, J. Solid State Chem. 177 (2004) 3058–3069.
[37] Y. Li, B. Gao, T. Wu, B. Wang, X. Li, Adsorption properties of aluminum magnesium mixed hydroxide for the model anionic dye Reactive Brilliant Red K-2BP, J. Hazard. Mater. 164 (2009) 1098–1104.
[38] R.R. Delgado, C.P. De Pauli, C.B. Carrasco, M.J. Avena, Influence of MII/MIII ratio in surface-charging behavior of Zn–Al layered double hydroxides, Appl. Clay Sci. 40 (2008) 27–37.
[39] I.D. Mall, V.C. Srivastava, N.K. Agarwal, Removal of Orange-G and Methyl Violet dyes by adsorption onto bagasse fly ash-kinetic study and equilibrium isotherm analyses, Dyes Pigm. 69 (2006) 210–223.
[40] Y. Guo, Z. Zhu, Y. Qiu, J. Zhao, Enhanced adsorption of acid brown 14 dye on calcined Mg/Fe layered double hydroxide with memory effect, Chem. Eng. J. 219 (2013) 69–77.
[41] A. Bouguettoucha, D. Chebli, T. Mekhalef, A. Noui, A. Amrane, The use of a forest waste biomass, cone of *Pinus brutia* for the removal of an anionic azo dye Congo red from aqueous medium, Desalin. Water Treat. 55 (2015) 1956–1965.
[42] X.J. Xiong, X.J. Meng, T.L. Zheng, Biosorption of C.I. Direct Blue 199 from aqueous solution by nonviable *Aspergillus niger*, J. Hazard. Mater. 175 (2010) 241–246.
[43] S.K. Milonjic, A consideration of the correct calculation of thermodynamic parameters of adsorption, J. Serb. Chem. Soc. 72 (2007) 1363–1367.
[44] A. Reffas, A. Bouguettoucha, D. Chebli, A. Amrane, Adsorption of ethyl violet dye in aqueous solution by forest wastes, wild carob, Desalin. Water Treat (in press), doi: 10.1080/19443994.2015.1031707.